

Mid–infrared and far–ultraviolet observations of the star–forming ring of M 31*

L. Pagani¹, J. Lequeux¹, D. Cesarsky², J. Donas³, B. Milliard³, L. Loinard⁴, and M. Sauvage⁵

¹ DEMIRM, Observatoire de Paris, 61 Avenue de l’Observatoire, F-75014 Paris, France

² Institut d’Astrophysique Spatiale, Bat. 121, Université Paris XI, F-91450 Orsay CEDEX, France

³ Laboratoire d’Astronomie Spatiale, BP8, Traverse du Siphon, F-13376 Marseille 12 CEDEX, France

⁴ IRAM, 300 Rue de la Piscine, Domaine Universitaire, F-38406 St Martin d’Hères CEDEX, France

⁵ SAp/DAPNIA/DSM, CEA-Saclay, F-91191 Gif sur Yvette CEDEX, France

Received 27 July 1998; accepted 23 August 1999

Abstract. We present mid–IR images of a $15' \times 15'$ field in the south–west part of the Andromeda galaxy M31 obtained with the ISOCAM camera ($6''$ pixels) on board ISO. These broad–band images complement spectro–imaging observations of smaller fields (Cesarsky et al. 1998). We also present a $20''$ resolution far–UV image of a larger field at 200 nm obtained with the balloon–borne telescope FOCA 1000. These images are inter–compared and also compared with H I, CO(1–0) and H α maps. The mid–IR emission as seen through wide–band filters centered at 7 and 15 μm is extremely well correlated with the distribution of neutral gas as shown by the H I and CO(1–0) maps, while the correlation is poorer with the distribution of the ionized gas seen through its H α emission. There is some correlation with the UV radiation, but it appears that the contribution of UV photons to the excitation of the carriers of the mid–IR emission is not dominant in most of M31. The spectro–imaging observations of Cesarsky et al. (1998) show that the mid–IR spectra of several regions of M31, two of which are in the presently studied area, are dominated by a strong emission band at 11.3 μm while emission in the other classical Aromatic Infrared Bands (AIBs) at 6.2, 7.7 and 8.6 μm is faint or absent. This result is precised, and we find that the mid–IR spectral variations are not clearly related to the UV radiation field. The present observations have important consequences on our understanding of excitation of the interstellar mid–IR emission in general. In particular, we conclude that like for M31, excitation in the Galactic cirruses may not be dominated by UV photons but rather by another mechanism which remains to be identified (visible

photons ?). The UV excitation appears to become important when the UV radiation density is of the order of 2 times that near the Sun.

Key words: galaxies: M31 - galaxies: ISM - dust, extinction - Infrared: ISM: lines and bands

1. Introduction

Most of the star formation in the Andromeda galaxy M31 is concentrated in a ring 10 kpc in radius, but even there the rate of star formation per unit area is modest. The far–IR emission of M31 is very faint for a spiral galaxy and its color temperature between 60 and 100 μm is also particularly low (Rice et al. 1988; Walterbos & Schwering 1987). The South–West part of the ring has been studied at many wavelengths, as summarized and discussed by Loinard et al. (1996, 1999). This ring is in fact the superimposition of several spiral arms which are difficult to disentangle from each other owing to the high inclination of the galaxy (77°). The most prominent of these arms, arm S4 (Baade 1963), is very similar in its CO line emission to the Carina spiral arm in our Galaxy; beyond a radius of about 8 kpc (the Solar circle) M31 and the Galaxy are comparable in their interstellar matter (ISM) content. We will see however that the star formation rate per unit surface is smaller than in the Milky Way even in the ring. It is considerably smaller in the more central parts.

We have imaged various parts of M31 with ISOCAM. Four $3' \times 3'$ fields have been observed with the Circular Variable Filters (CVF) in the wavelength range 5.15 to 16.5 μm (Cesarsky et al. 1998). The CVF spectra obtained are unlike anything that has been observed before from the interstellar medium in our Galaxy and in other

Send offprint requests to: james.lequeux@obspm.fr

* Based on observations with ISO, an ESA project with instruments funded by ESA member states (especially the PI countries: France, Germany, the Netherlands and the United Kingdom) and with the participation of ISAS and NASA.

galaxies. The spectra of the central region and of a region in the bulge show a strong, broad emission band at $11.3\ \mu\text{m}$ while the other Aromatic Infrared Bands (AIBs) at 6.2 , 7.7 and $8.6\ \mu\text{m}$ are not or only marginally detected. No observation of M31 in the $3.3\ \mu\text{m}$ AIB exists. Note that a recent ISOCAM filter imaging of the spiral galaxy NGC 7331 (Smith 1998) appears to show a similar situation in the bulge of this galaxy. The emission of the bulge of NGC 7331 in the LW8 ($10.7\text{--}12.0\ \mu\text{m}$) filter is strong compared to its emission in filters around $7\ \mu\text{m}$ (after the stellar continuum contribution is subtracted). In the bulge of M31 (Cesarsky et al. 1998), the $11.3\ \mu\text{m}$ band has a spatial distribution very different from that of the stars and is therefore emitted by interstellar rather than circumstellar material. The spectrum obtained in a quiet region of the star-forming ring is similar to those obtained near the center, while the spectrum of an active star-forming region is more comparable to usual Galactic or extragalactic AIB spectra, although the $11.3\ \mu\text{m}$ band is still particularly strong compared to the other bands.

In the present paper, we report the results of ISOCAM observations of a $15'\times 15'$ field in the SW side of the ring made through the LW2 ($5.0\text{--}8.0\ \mu\text{m}$) and the LW3 ($12.0\text{--}18.0\ \mu\text{m}$) filters. These observations were made in the guaranteed time of ISO as parts of a systematic program on interstellar matter in the Galaxy, the Magellanic Cloud, M 31, M 33 and more distant galaxies, in particular a complete sample of galaxies in the Virgo cluster (Boselli et al. 1997, 1998). The CVF observations mentioned before show that these filters were not the best choices for M31. The LW8 ($10.7\text{--}12.0\ \mu\text{m}$) filter which encompasses the $11.3\ \mu\text{m}$ band would have been very useful, but it was too late to obtain further observations before the end of the life of ISO. The filter observations of the central regions of M31 will be described in a forthcoming paper.

We also present observations of the same part of M31 in the far-UV at $200\ \text{nm}$. These data were obtained with the balloon-borne telescope FOCA 1000 of the Laboratoire d'Astronomie Spatiale in Marseille, and are very complementary to the mid-IR observations.

Sect. 2 describes the ISO observations and their reductions. Sect. 3 is devoted to the observations in the far-UV and their reductions. Sect. 4 compares the morphology of the different emissions observed from far-UV to radio wavelengths. Sect. 5 discusses the excitation of the mid-IR emission and Sect. 6 compares the mid-IR emissions in the two ISOCAM filters LW2 and LW3. Sect. 7 compares the mid-IR emission in LW2 and LW3 with the CVF observations. Sect. 8 contains the conclusions.

2. ISO observations and data reduction

The mid-infrared observations have been made with the 32×32 element camera (CAM) on board of the ISO satellite, (see Cesarsky et al. 1996 for a complete description). The pixel size was $6''\times 6''$. We obtained for each filter

(LW2 and LW3) a square 9×9 -step raster map with a shift (then overlap) of 16 pixels between successive positions. The integration time was 2.1 seconds. 50 exposures were eliminated at the beginning of each observation in order to insure a better stabilization of the detector, which shows remanence of its previous illumination history. 20 2.1s exposures were added for each raster position. The total useful integration time was about 1 hour per filter.

Data reduction was accomplished using the CAM Interactive Analysis (CIA) software¹. Most of this analysis is described by Starck et al. (1999). The map at each wavelength was dark-current subtracted using the dark frame model appropriate to the epoch of the observations. It was then flat-fielded using library flats. Automatic softwares were used to detect and eliminate the parts of the record affected by glitches due to the impact of charged particles, and also to correct for the transient response of the detector when submitted to changes in incident flux. The new transient correction described by Coulais & Abergel (1998) has been applied, yielding considerable improvements with respect to the previous method implemented in the CIA software. In particular, the photometric accuracy of our maps is now believed to be of the order of 10 %. Corrections for field distortion have been applied to images at each position before combining them in a raster. The final raster images are of excellent cosmetic quality. Their resolution is limited by the $6''$ sampling at short wavelengths and by diffraction at longer wavelengths, reaching $8''$ at $15\ \mu\text{m}$. A constant background corresponding mostly to the zodiacal light, measured in apparently blank regions of the maps (bottom left and top right corners of Fig. 1) has been subtracted from the LW2 and the LW3 images. The significance of this offset will be discussed later in Sect. 4.

3. Far-UV observations and reductions

Far-UV observations of M31 have been made in October 1985 during a balloon flight of the FOCA 1000 ultraviolet telescope of the Laboratoire d'Astronomie Spatiale. This telescope has a diameter of 40 cm and a focal length of 1000 mm. It is equipped with a UV camera consisting of a microchannel plate and a Kodak IIAO photographic film. The field of view is $2^\circ 3'$ and the angular resolution is $20''$. The bandpass is $\sim 15\ \text{nm}$ wide centered at $\lambda_0 = 200\ \text{nm}$. This facility is described in Milliard et al. (1991). Six 200 seconds exposure frames centered on the guide star HD 3431 have been obtained. Each frame was digitized with a PDS 1010s densitometer with a slit size of $25\ \mu\text{m} \times 25\ \mu\text{m}$ and processed by an automatic sequence of programs (Moulinec 1989) designed to convert the photographic density into a linear intensity scale, to correct for

¹ CIA is a joint development by the ESA Astrophysics Division and the ISOCAM Consortium led by the ISOCAM PI, C. Cesarsky, Direction des Sciences de la Matière, C.E.A., France

the detector background and for local differences in sensitivity of the microchannel plate. They have then been digitally summed to form the final image. The resulting 1640×1640 pixel image is equivalent to a single exposure of 1200 s. This image has been corrected for the distortion of the optics to an accuracy $\simeq 2''$ and recentered using stars of the Digital Sky Survey to produce Fig. 3 and Fig. 8. The photometric zero point has been determined on the basis of 11 stars in common with the previous SCAP2000 observation (Donas et al. 1987). This calibration gives fluxes 0.1 mag. fainter than the ANS photometry of several fields of the SW part of M 31 (Israël et al. 1986), clearly within the uncertainties of both calibrations. The random error on the fluxes is of the order of 0.35 mag. (Donas et al. 1991).

4. Morphology of the mid-IR emission and other components of M 31

Figure 1 is the LW2 ($5.0\text{--}8.0 \mu\text{m}$) map superimposed over the Digital Sky Survey (DSS) image clipped in order to show only stars. A number of Galactic stars are visible in the LW2 image and have been used to recenter this image. The LW3 ($12.0\text{--}18.0 \mu\text{m}$) image (not shown in full but see Fig. 14, 15 and 16 later) has been itself recentered on the LW2 one, having many features in common. The position accuracy after recentering is of the order of half a pixel ($3''$), similar to that of the UV map.

Figure 2 is similar to Fig. 1 except that the DSS image shows fainter levels and that the LW2 image is presented as contours. It shows the excellent correspondence of the near-IR emission with the distribution of large dust grains as revealed by the absorption marks in front of the stellar emission of M 31. The LW3 image being very similar to the LW2 one shares this property. A similarity between the LW3 emission and the distribution of big dust grains has also been seen and discussed by Block et al. (1997) in the case of M 51. Figure 2 also shows that the contribution of stellar photospheres that dominate the visible image is negligible in the LW2 filter, at least for the ring of M 31. In the central parts of M 31 discussed in a future paper, this is no more true.

Figure 3 is the far-UV (200 nm) map (see Sect. 3).

Figures 4 and 5 show the superimpositions of the LW2 map over the H I and CO maps respectively. The emission seen in the LW2 filter follows extremely well the distribution of the interstellar matter as seen in the H I and the CO lines. As we will see later, it is likely that this emission is dominated by the AIBs at 6.2 , 7.7 and $8.6 \mu\text{m}$. These bands are faint in M 31 but the LW2 emission is also quite faint. Tran (1998) has shown that in general the mid-IR bands are well correlated with H I, in particular in photodissociation regions. On Fig. 6, we plot the the intensity in the LW2 filter as a function of the total column density of neutral gas $N(\text{H}) = N(\text{H I}) + 2N(\text{H}_2)$,

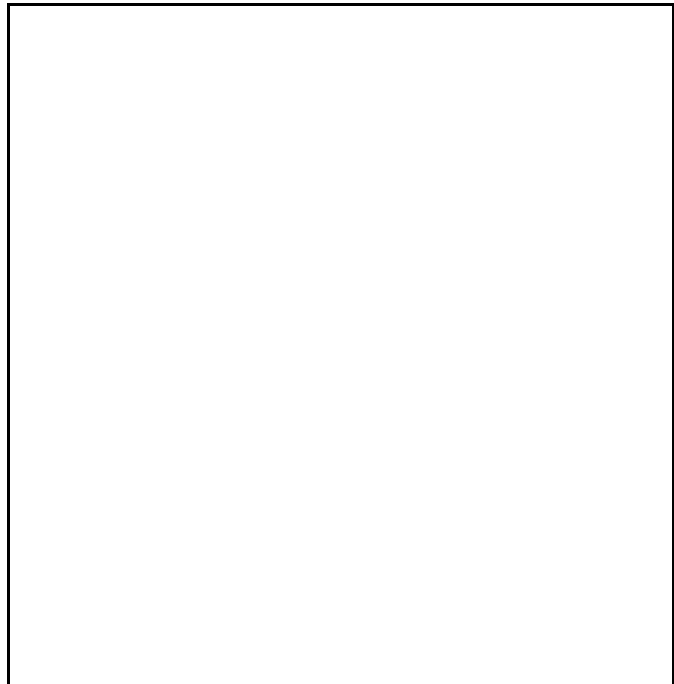


Fig. 1. Map of the SW portion of the ring of M 31 in the LW2 filter ($5.0\text{--}8.0 \mu\text{m}$) (grey scale), superimposed on the DSS image, clipped such as to show only the stars. Coordinates are for J2000. The grey scale unit is 1 mJy per $6''$ pixel, in decimal logarithmic scale. The two $3'$ fields observed with the Circular Variable Filters (CVF) of ISOCAM are indicated by two squares. Field **c** covers an active star-forming region while Field **d** corresponds to a quiet region dominated by molecular gas. Note the rich OB association NGC 206 to the West of Field **d**. This labelling makes reference to Cesarsky et al. (1998)

$N(\text{H}_2)$ being derived from the intensity of the CO(1–0) line by:

$$N(\text{H}_2) = 1.5 \cdot 10^{20} I(\text{CO}) \text{ mol. cm}^{-2} (\text{K km/s})^{-1}$$

The conversion factor, adapted from Dumke et al. (1997) and Digel et al. (1996), is uncertain by at least 50 %. Our choice is in agreement with the factor $1.2 \cdot 10^{20} \text{ mol. cm}^{-2} (\text{K km/s})^{-1}$ found by Neiminger et al. (1998). The result of the correlation is not very sensitive to its value because most of the $45''$ pixels used for building Fig. 6 are dominated by H I. Note that there is an error in the H I column densities given by Loinard et al. (1996) which is corrected here and in Loinard et al. (1999). A least-square fit to the points of Fig. 6 yields:

$I(\text{LW2}) = (2.24 \pm 0.06) \cdot 10^{-22} N(\text{H}) - 0.23 \text{ mJy pixel}^{-1} (\text{H-atom cm}^{-2})^{-1}$ with a correlation coefficient $r^2 = 0.79$. The non-zero intercept is probably not physically significant. It may be due to the uncertainty on the base level of the LW2 map and perhaps also of the H I map. From the column density of H I and H_2 at the points chosen to determine the LW2 background (see Sect. 2), we expect from the correlation slope a flux in LW2 of 0.3 mJy/pixel instead of the assumed value of zero at these points. After

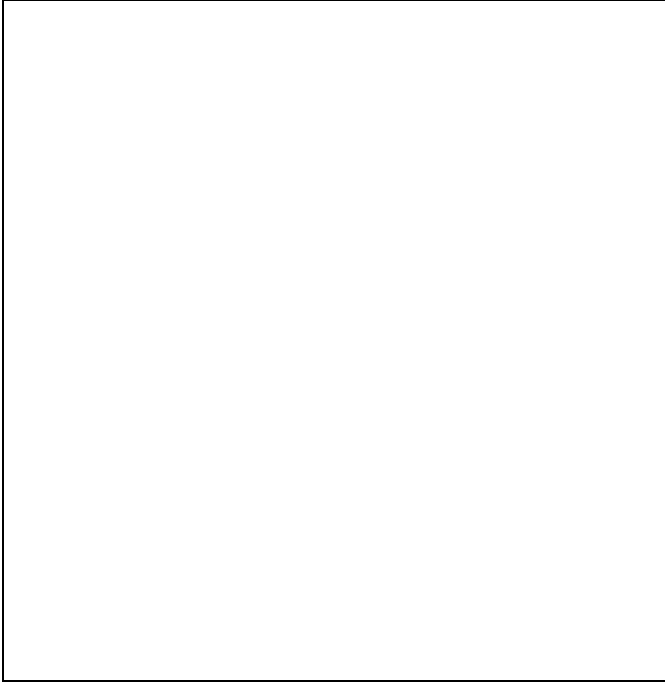


Fig. 2. Map of the SW portion of the ring of M 31 in the LW2 filter (5.0–8.0 μm) (contours), superimposed on the positive, full-sensitivity DSS image. Coordinates are for J2000. The first contour level is 0.4 mJy per $6''$ pixel then the contours are from 1 to 6 mJy/pixel by steps of 0.5 mJy/pixel. The levels might be too low by 0.3 mJy/pixel (see Sect. 4). Note the excellent correspondence of the near-IR emission with the absorption marks in front of the stellar emission of M 31

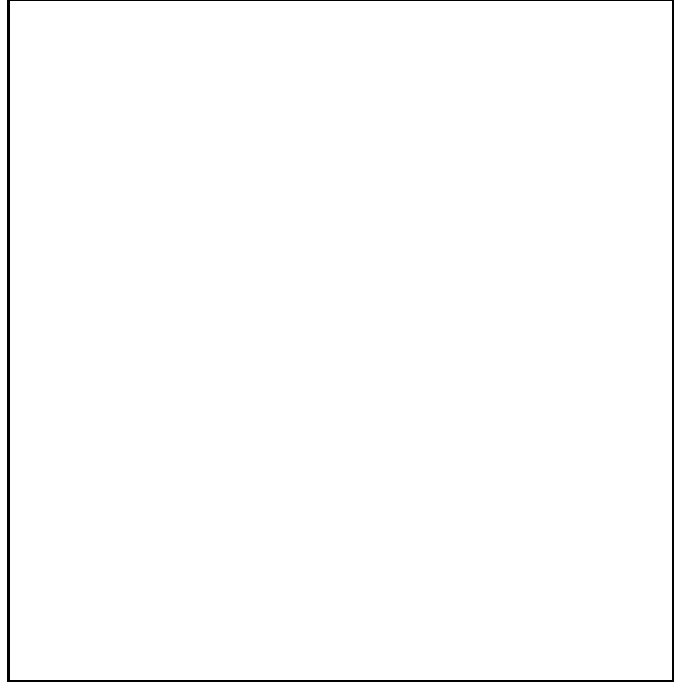


Fig. 3. Map of the SW portion M 31 in the far-UV at 200 nm obtained with the FOCA-1000 balloon-borne telescope. The angular resolution is $20''$. The color scale unit is $2.1 \cdot 10^{-17} \text{ erg cm}^{-2} \text{ s}^{-1} \text{ \AA}^{-1} \text{ arcsec}^{-2}$. The background level as measured outside the galaxy is 0.116 unit. It has no physical significance. The UV emission is a tracer of recent ($< 3 \cdot 10^8 \text{ yr}$) star formation but radiation also results from scattering by dust of the stellar UV emission

the corresponding correction, this would yield an actual intercept of 0.07 mJy/pixel which is negligible. The slope of the relation is similar within the fairly large errors (at least 30 %) to that for the Galactic cirrus as derived from a combination of the results obtained by Boulanger et al. (1996), Onaka et al. (1996) and Reach & Boulanger (1998).

Figures 7 and 8 show superimpositions of the LW2 map over the $\text{H}\alpha$ and far-UV maps respectively. The correlation between the mid-IR emission and $\text{H}\alpha$ is very poor and there is almost no correlation with the far-UV radiation. There are however mid-IR peaks associated with H II regions as depicted by $\text{H}\alpha$. In our Galaxy, the emission at 5–8 μm (the wavelength range of the LW2 filter) is strong in photodissociation regions (PDRs) at the interfaces between H II regions and molecular clouds (M 17: Cesarsky et al. 1996b; Orion bar: Cesarsky et al. 1999) and at the surfaces of molecular clouds illuminated by UV radiation (reflection nebulae like NGC 7023: Cesarsky et al. 1996a). There is also emission from the more diffuse interstellar gas (see e.g. Abergel et al. 1996). However we do not know well the relative importance of these various sources at the scale of a galaxy. Our observation of M 31 gives a clear information on this point. The presence

of peaks associated with H II regions probably indicates mid-IR emission from interfaces, but there is some ambiguity here because there is also much ISM close to the H II regions. In any case, the mid-IR emission of the interfaces cannot be a large fraction of the total, since there is much diffuse mid-IR emission in M 31 far from $\text{H}\alpha$ emission regions. We will see later (fig. 11) that only very few localized regions in M 31 have a LW3/LW2 intensity ratio (in Jy) larger than 1, a characteristic of strong PDRs.

Particularly interesting is the vicinity of the main OB association of M 31, NGC 206 = OB 78 (see Fig. 1). The stellar winds and perhaps supernova explosions in this association have eroded a hole in the interstellar medium while triggering some secondary star formation in the resulting shell (Fig. 1 and 7). The UV emission of the association itself is very strong (Fig. 3 and 8, see also Hill et al. 1993). The Lyman continuum photons from the OB stars of this association (Massey et al. 1995 and references herein) ionize the inner shell as it can be seen clearly in $\text{H}\alpha$ (Fig. 7). Still the mid-IR flux is not higher in this region than in inactive regions with similar column densities of gas. *This confirms that the main factor which determines the mid-IR flux is the amount of gas, except in the immediate vicinity of regions where massive stars have just*

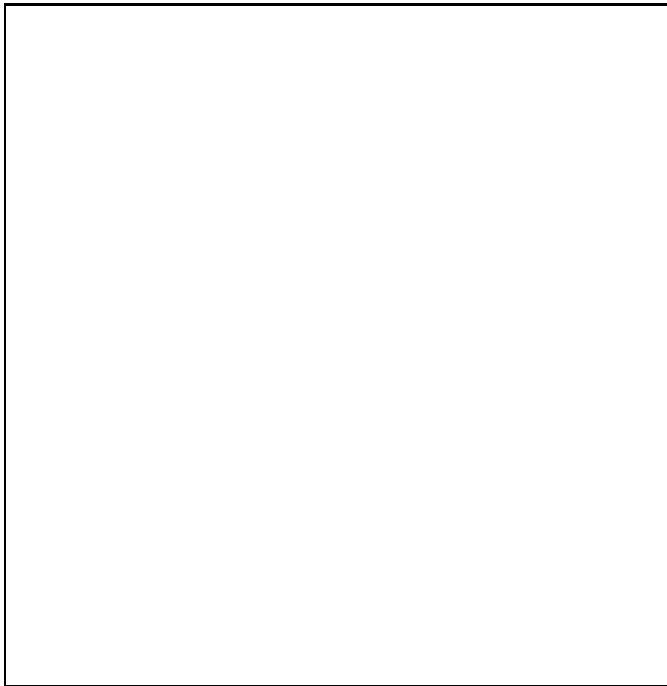


Fig. 4. Map of the SW portion of the ring of M 31 in the LW2 filter (5.0–8.0 μm) (color). The color scale unit is 1 mJy per 6'' pixel, and the scale is truncated at 3 units to obtain a better display of the faint emission. The contours indicate the 21-cm line integrated intensity, from data in Brinks & Shane (1984): contours with levels from 1000 to 3500 K km/s^{-1} in steps of 500 K km/s^{-1} . The 1000 K km/s^{-1} contour is in red for clarity. Note that there is an error in the level specification in Loinard et al. (1996). The angular resolution of the 21-cm map is $24'' \times 36''$. Note the excellent correlation between mid-IR and H I emissions, in particular at the faintest levels. The yellow boxes delineate regions for which the mean UV intensity has been evaluated, as discussed in the text

formed. Several such regions are well visible in the shell around NGC 206 (Fig. 7), each one with its own mid-IR peak.

We conclude from these morphological considerations that in the ring of M 31 the emission in the LW2 filter (5.0–8.0 μm) is dominated by the diffuse ISM bathed in the general interstellar field. This confirms the result of the analysis of IRAS data from the solar neighbourhood by Boulanger & Pérault (1988). They showed that most of the interstellar infrared emission comes from ISM not associated with current star formation. Their result actually applies to the far-IR emission but since there is a good correlation between the emission in the 12 μm IRAS filter and that in the filters at longer wavelengths it is likely to be true for the mid-IR emission as well.

5. The excitation of the mid-IR emission in M 31

The mid-IR band emission is generally considered to be excited by individual UV photons that transiently heat

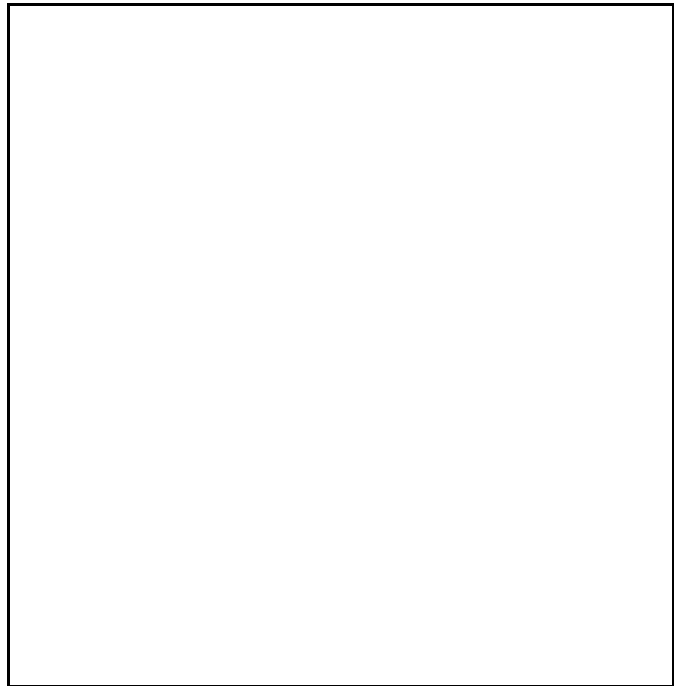


Fig. 5. Map of the SW portion of the ring of M 31 in the LW2 filter (5.0–8.0 μm) (grey scale), superimposed on the CO(1–0) line map from Loinard et al. (1999): contour levels from 2 to 8 K km/s^{-1} in steps of 1 K km/s^{-1} . The angular resolution of the CO map is $45''$. For clarity, the LW2 image is plotted in a decimal logarithmic scale (unit: 1 mJy per 6'' pixel). Note the good correlation between the distributions of H I (Fig. 4), CO and mid-IR

these particles to very high temperatures. However Uchida et al. (1998) found a “normal” Galactic AIB spectrum in the reflection nebula vdB 133, which is illuminated by a relatively cool binary star, and noticed that this poses a problem for the emission mechanism of the mid-IR bands. This is amply confirmed by our observations of M 31, as we will demonstrate now.

The correlation between the mid-IR and the far-UV emission in M 31 (Fig. 8) is apparently extremely poor. The lack of correlation must be due to some extent to the strong extinction in the gas and dust ring, given the large inclination of M 31 on the line of sight. This extinction affects very much the UV radiation, but little the mid-IR.

To get rid of the problem of extinction, we compare the ratios along the same 21-cm line brightness isophote of 1000 K km/s^{-1} on each side of the 10 kpc ring (see Fig. 4, yellow boxes 1 and 2). The column density of H atoms in H_2 is estimated to be $4.5 \cdot 10^{20} \text{ cm}^{-2}$ in box 1 and $3.8 \cdot 10^{20} \text{ cm}^{-2}$ in box 2 compared to $1.8 \cdot 10^{21} \text{ cm}^{-2}$ for H I. In the Appendix we give estimates of the far-UV/visible interstellar intensity ratio per unit wavelength in various parts of M 31. We find $I_\lambda(200 \text{ nm})/I_\lambda(550 \text{ nm}) \simeq 0.20$ on the outer side (box 2) which is brighter in UV (see Fig. 8)

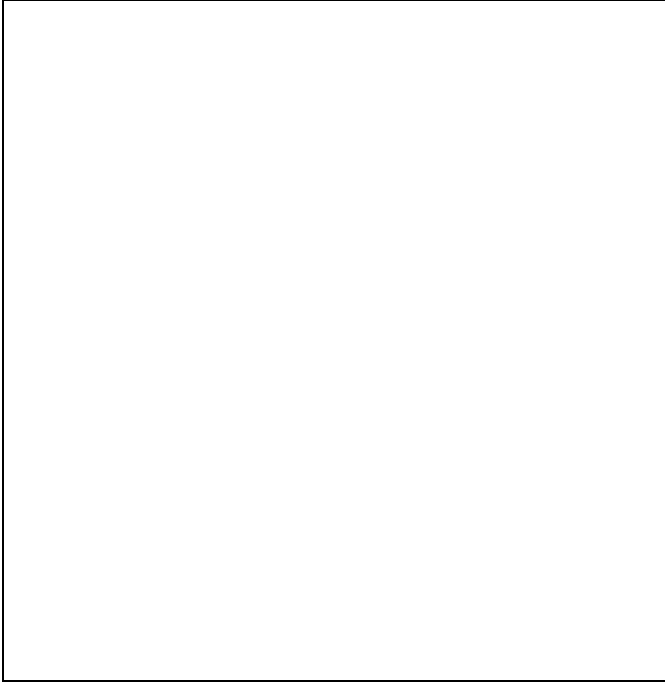


Fig. 6. The intensity in the LW2 filter (5.0–8.0 μm) as a function of the total column density of neutral gas $N(\text{H})$ in the SW region of M31. The size of the pixels used for building this figure is $45''$. The correlation is excellent. The intercept is discussed in the text

and 0.05 on the inner side (box 1). This difference cannot be due to extinction since the column densities of interstellar matter are the same for the two boxes. The intensity in the LW2 filter is almost the same for the two regions (respectively 0.23 and 0.28 mJy/pixel plus a possible offset of about 0.3 mJy/pixel). This example shows beyond any doubt that the mid-IR intensity is almost independent of the UV radiation field in the observed region of M31. This suggests that the AIBs in M31 are in general not primarily excited by the far-UV photons.

The far-UV/visible interstellar intensity ratios on both sides of the ring of M 31 are affected by the same amount of extinction and a model is required if one wishes to obtain dereddened ratios. This is done in the Appendix where we show that the dereddened ratios are roughly 1.55 times larger than the observed ones. For comparison, $I_\lambda(200 \text{ nm})/I_\lambda(550 \text{ nm}) \simeq 0.65$ in the Solar neighbourhood. Thus on both sides of the ring the $I_\lambda(200 \text{ nm})/I_\lambda(550 \text{ nm})$ ratio is smaller than near the Sun, and it is clear that in this case the UV radiation has a negligible effect to excite the mid-IR emission. In the Appendix, we also show that the UV/visible ratio in the reflection nebula vdB 133 observed by Uchida et al. (1998) is of the order of 0.4, slightly smaller than in the Solar neighbourhood but definitively larger than in quiescent regions of the ring of M31. Thus our observations of M31 yield an even more convincing case for the fact that excitation of the bearers of the AIBs

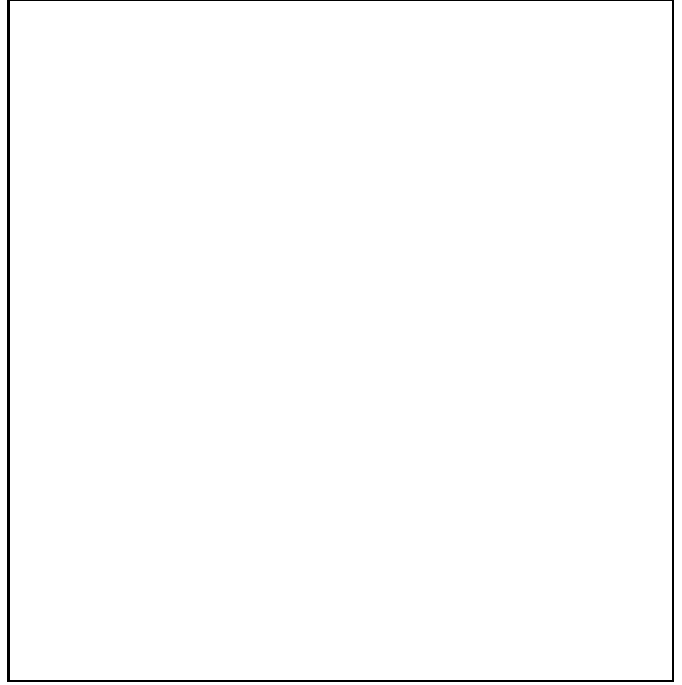


Fig. 7. Map of the SW portion of the ring of M31 in the LW2 filter (5.0–8.0 μm) (clipped grey scale), superimposed on an image (contours) kindly communicated by N. Devereux (see Devereux et al. 1994). The $\text{H}\alpha$ contours are approximately $5 \cdot 10^{-16}$, 10^{-15} and $3 \cdot 10^{-15} \text{ erg cm}^{-2} \text{ s}^{-1}$ per $2''$ pixel. The unit for the LW2 image is 1 mJy per $6''$ pixel. The $\text{H}\alpha$ emission is limited to the outer side of the ring of interstellar matter as defined by the H I, CO and mid-IR emission. $\text{H}\alpha$ emission surrounds the association NGC 206

(PAHs?) does not require UV radiation. Excitation might be by visible photons. In this case the emitters, if they are PAHs, must be smaller than usually assumed since single-photon excitation by photons some 5 times less energetic than considered usually should bear them transiently to a temperature of several hundred degrees. Alternatively, the AIB excitation may be linked in some way to H I given the excellent correlation between mid-IR and H I. A possibility could be that formation of H_2 molecules by combination of H atoms on the AIB carriers supplies their heating (Papoular 1999). However it is easy to see that this mechanism fails by two orders of magnitude in the case of Galactic PDRs and cirrus (F. Boulanger, private communication). This is probably also the case for M31.

There is however an underlying correlation between the mid-IR flux *per H atom* and the UV flux. This is illustrated by Fig. 9, where we have plotted the intensity in the LW2 band normalized by the total column density of the neutral gas $N(\text{H})$ as a function of the intensity at 200 nm. The intensity in the LW2 band has been corrected from the non-zero intercept seen on Fig. 6 by adding to it 0.3 mJy/pixel before dividing by $N(\text{H})$ (see Sect. 4). From Fig. 9 we see that UV excitation becomes important only

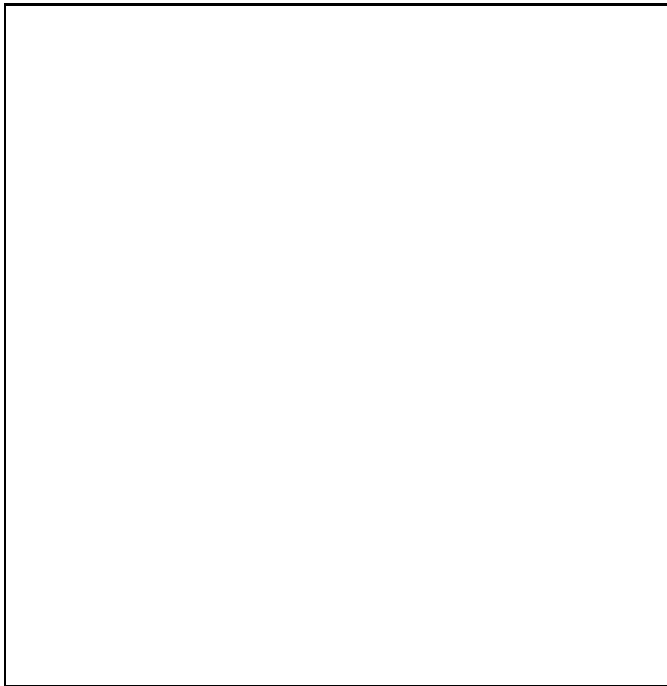


Fig. 8. Map of the SW portion of the ring of M 31 in the the far-UV at 200 nm (contours) superimposed on the LW2 filter (5.0–8.0 μm) map (color). The UV contours are at 0.15, 0.2, 0.3, 0.4, 0.5, 1.0 and 2.0 in units of $2.1 \cdot 10^{-17} \text{ erg cm}^{-2} \text{ s}^{-1} \text{ \AA}^{-1} \text{ arcsec}^{-2}$. The background is at 0.116 unit. The LW2 filter color scale unit is 1 mJy/pixel. It is truncated at 3 units for clarity. A few OB associations give a very strong UV emission, in particular NGC 206. Most of the diffuse UV emission comes from outside the ring of interstellar matter as defined by the H I, CO and mid-IR emission. The UV within the ring is affected by extinction. The extended UV emission is probably in part light scattered by dust in the diffuse ISM

above an uncorrected surface brightness $I_{UV} \simeq 2 \cdot 10^{-18} \text{ erg cm}^{-2} \text{ s}^{-1} \text{ \AA}^{-1} \text{ arcsec}^{-2}$. The least-square regression line has a slope of $10^{-22} \text{ mJy pixel}^{-1} \text{ cm}^{-2} \text{ per } 10^{-18} \text{ erg cm}^{-2} \text{ s}^{-1} \text{ \AA}^{-1} \text{ arcsec}^{-2}$ for $I_{UV} > 2 \cdot 10^{-18} \text{ erg cm}^{-2} \text{ s}^{-1} \text{ \AA}^{-1} \text{ arcsec}^{-2}$, mostly determined by a few UV-bright regions. This would determine the amount of excitation due to the UV radiation if one could correct the UV flux for extinction, a very difficult task for UV-bright regions. In any case, the extinction correction is likely to decrease strongly the slope of the regression line.

The weakness of the mid-IR/UV correlation has important consequences. It seems to imply that at low UV intensities UV excitation of the LW2 emitters is unimportant with respect to another excitation mechanism that remains to be determined. The dereddened UV surface brightness corresponding to the threshold for UV excitation is of the order of $10^{-17} \text{ erg cm}^{-2} \text{ s}^{-1} \text{ \AA}^{-1} \text{ arcsec}^{-2}$ (see Appendix). It is easy from data in the Appendix to calculate that the true (unreddened) UV surface brightness of the Galactic disk near the Sun, assumed to be seen

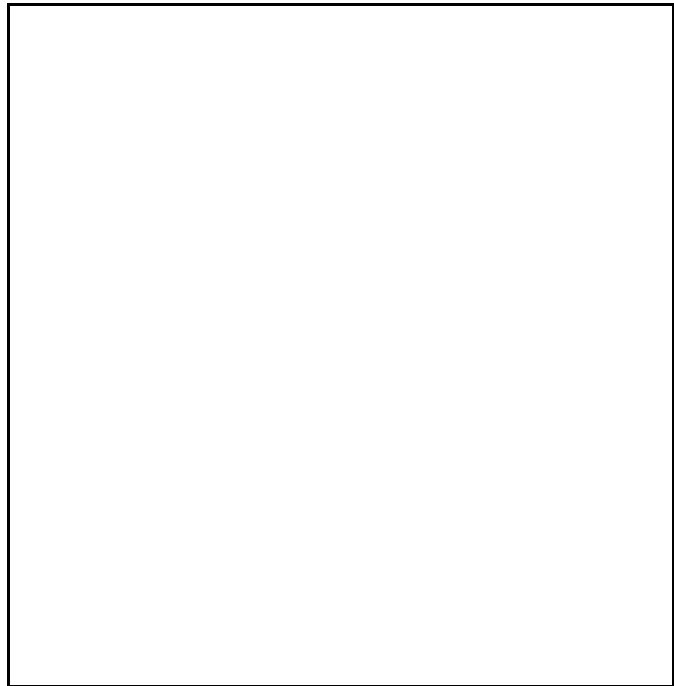


Fig. 9. The intensity in the LW2 filter (5.0–8.0 μm) normalized by the total column density of neutral gas in the SW region of M 31, as a function of the uncorrected intensity of the far-UV light at 200 nm. The size of the pixels used for building this figure is $45''$. There is only a weak correlation between the LW2 flux per H atom and the intensity of the UV field which appears above a threshold value of $\simeq 2 \cdot 10^{-18} \text{ erg cm}^{-2} \text{ s}^{-1} \text{ \AA}^{-1} \text{ arcsec}^{-2}$

from the same inclination of 77° as M 31, would be $\simeq 5 \cdot 10^{-18} \text{ erg cm}^{-2} \text{ s}^{-1} \text{ \AA}^{-1} \text{ arcsec}^{-2}$ at 200 nm. This is less than the above threshold and suggests that the mid-IR emission of the Galactic cirruses is also only marginally excited by UV photons. This may explain why the ratio between the LW2 intensity and $N(\text{H})$ is so similar in M 31 and for Galactic cirruses in spite of the difference in their UV fluxes. A UV radiation density 2 times larger than that near the Sun appears to be needed for UV excitation to become appreciable in the disks of M 31 and of the Galaxy.

6. The LW3(12.0–18.0 μm)/LW2(5.0–8.0 μm) band ratio

In the previous sections, we have only discussed the LW2 observations. The LW3 (12.0–18.0 μm) image (not shown) is at first sight very similar to the LW2 (5.0–8.0 μm) one. We show on Fig. 10 the pixel-to-pixel correlation between the brightnesses in the two maps. A Hanning smoothing has been applied to both the LW2 and the LW3 images in order to obtain similar angular resolutions at both wavelengths. The correlation is excellent. The two-dimension regression line gives

$$I(\text{LW3}) = 0.82 I(\text{LW2}) - 0.10$$

with a correlation coefficient $r^2 = 0.72$. The units are mJy/pixel for both intensities. The overall similarity between the LW3, the LW2 map and the neutral gas indicates that the excitation mechanisms in the two wavelengths ranges must be related to each other and to the neutral ISM.

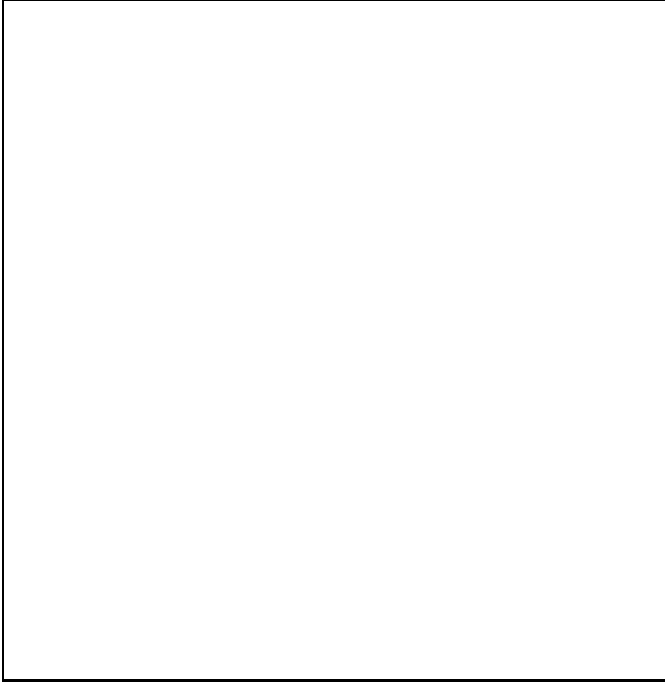


Fig. 10. The intensities measured in the LW3 (12.0–18.0 μm) as a function of the intensities in the LW2 (5.0–8.0 μm) filter. A Hanning smoothing has been applied to the LW2 and LW3 maps in order to obtain similar angular resolutions at both wavelengths. Notice the bifurcation of the correlation at large intensities. The deviating points forming an almost horizontal sequence below the main correlation correspond to stars

The $I(\text{LW3})/I(\text{LW2})$ ratio is surprisingly similar to that in more “normal” galaxies. For comparison, in the region of the ρ Ophiuchi cloud mapped by Abergel et al. (1996) this ratio is between 0.6 and 1.0. It is somewhat larger than 0.8 everywhere in M 51 (Sauvage et al. 1996) or in NGC 6946 (Helou et al. 1996). Integrated over whole normal galaxies, the $I(\text{LW3})/I(\text{LW2})$ ratio is always larger than 0.5 except for a few irregular galaxies (Boselli et al. 1997, 1998).

In spite of the overall similarity between the LW2 and LW3 maps, there are interesting differences. The existence of localized regions where the LW3/LW2 intensity ratio deviates from the mean at relatively large intensities is visible on Fig. 10. The points with a low LW3 intensity with respect to the LW2 one correspond to stars. For these points one has approximately $I(\text{LW3})/I(\text{LW2}) \simeq 0.25$, as expected for a Rayleigh–Jeans blackbody law. There are

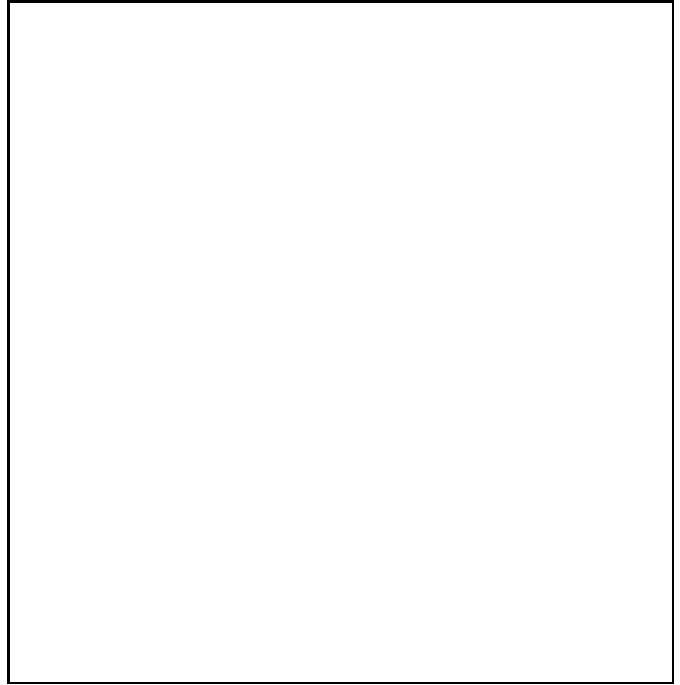


Fig. 11. A partial map of the ratio between the intensities measured in the LW3 (12.0–18.0 μm) and in the LW2 (5.0–8.0 μm) filters. A Hanning smoothing has been applied to the LW2 and LW3 maps in order to improve the signal-to-noise ratio and to have approximately the same angular resolution at both wavelengths. Only the points for which the intensities are larger than 4 times the r.m.s. noise have been used. The $\text{H}\alpha$ map is superimposed (contours from $5 \cdot 10^{-16}$ to $5 \cdot 10^{-15}$ by steps of $5 \cdot 10^{-16}$ $\text{erg cm}^{-2} \text{s}^{-1}$ per $2''$ pixel). Only a part of the total field is depicted, showing a few “hot spots” with a large LW3/LW2 intensity ratio. There are no such conspicuous hot spots in the rest of the surveyed region

also a few points for which $I(\text{LW3})/I(\text{LW2})$ is large. Fig. 11 is an enlarged map of the intensity ratio in a part of the M 31 ring, on which a few such “hot spots” can be seen. A possible explanation is that if the radiation field becomes large enough, then very small 3-dimensional grains contribute to the emission in the LW3 filter. This has been discussed e.g. by Cesarsky et al. (1996b). Curiously, the hot spots are close to H II regions, but not coinciding with them. It is likely that we see the interfaces between the H II regions and molecular clouds, or material heated by young, massive stars embedded in molecular clouds. The angular resolution of our maps, in particular the CO one, does not allow to check this point. Near-IR observations will be very useful to ascertain the nature of the hot spots.

7. The nature of the emission in the LW2 and LW3 filters: comparison with CVF observations

CVF observations are available for Fields c and d of Fig. 1. Their global spectrum is shown in Fig. 3c and 3d of Cesarsky et al. (1998) respectively. Field d is a quiescent

region with little star formation and its spectrum is dominated by a broad band centered at $11.3 \mu\text{m}$, with only marginal emission in the 6.2 , 7.7 and $8.8 \mu\text{m}$ bands. We have built a map of the $11.3 \mu\text{m}$ feature in this field. It shows some relation with the LW2 and LW3 maps, but it is very noisy due to the faintness of the emission and no clear conclusion can be extracted from it. Field c is a more active region and its mid–IR emission is stronger. Its global CVF spectrum shows all the classical AIBs although the $11.3 \mu\text{m}$ is relatively very strong. We will now discuss its mid–IR emission in detail.

We performed a further reduction of the CVF observation of Field c. It has been reprocessed with the new transient correction algorithm (Coulais & Abergel 1998), and recentered using a star which is visible on the LW2 map and in the short–wavelength channels of the CVF. We then defined a background emission spectrum using pixels considered as free from emission in the AIBs. This spectrum, which is essentially the zodiacal light spectrum, has been subtracted from the spectra of the individual pixels in order to produce differential spectra showing more clearly the AIBs. Note that the continuum is partly lost in this process because the response of the detector to the zodiacal light is not uniform due to reflections between the CVF and the detector, and not yet well calibrated. We have then produced maps in the $6.2 \mu\text{m}$ band and in the $11.3 \mu\text{m}$ one, as well as average differential spectra in the regions emitting sufficiently strongly in these bands.

Figure 12 compares the average differential CVF spectra obtained with three different selections of pixels: those with a sufficiently strong emission at $6.2 \mu\text{m}$ but a weak emission at $11.3 \mu\text{m}$, those pixels in the opposite case and those pixels with a relatively strong emission at both 6.2 and $11.3 \mu\text{m}$. This illustrates the diversity of spectra found in the field, which go from “normal” AIB spectra similar to those in our Galaxy to spectra with a relatively strong, broad $11.3 \mu\text{m}$ feature and very little emission in the 6.2 , 7.7 and $8.6 \mu\text{m}$ bands.

Figure 13 is the CVF map in the $6.2 \mu\text{m}$ feature, superimposed over the LW2 map. We see on this figure that the two distributions are similar, with a relatively strong peak in the direction of the H II region PAV78 159 (Pellet et al. 1978) = BA 1-313 (Baade & Arp 1964). This shows that the emission in the LW2 filter is due to the $6.2 \mu\text{m}$ and probably also the $7.7 \mu\text{m}$ AIBs, and possibly to an associated continuum. It is unfortunately not possible at the present stage to simulate the flux in the LW2 filter from the CVF data, due to the partial loss of the continuum level in the CVF reductions.

Figure 14 contains the CVF map in the $11.3 \mu\text{m}$ feature, superimposed over the LW3 map. The LW3 map is qualitatively similar to the LW2 map displayed on Fig. 13, the most conspicuous difference being the expected absence of the Galactic star in the LW3 map. These differences can be seen on the partial map of Fig. 16. Both filter maps show only a loose similarity to the $11.3 \mu\text{m}$ band

map. We also display on the right of the figure differential average spectra for the pixels showing emission in the $11.3 \mu\text{m}$ band, in three strips of the CVF field. This shows that the $11.3 \mu\text{m}$ emission regions of the lower–left band, which are not conspicuous in the filter maps, are real. Clearly the LW3 emission has little to do with the $11.3 \mu\text{m}$ feature (note that this feature is *not* included in the passband of the LW3 filter). This emission is essentially a continuum. Usually one attributes this continuum to the emission of very small grains heated in semi–equilibrium by the absorption of (mainly UV?) photons (Désert et al. 1990; Cesarsky et al. 1996b). However this interpretation is obviously disputable here.

It is interesting to precise in this respect that the contribution of the $11.3 \mu\text{m}$ feature to the emission in the IRAS $12 \mu\text{m}$ filter (8.0 – $15.0 \mu\text{m}$) is minor. The average IRAS brightness at $12 \mu\text{m}$ in Field c is $\simeq 0.7$ mJy per $6''$ pixel from Walterbos & Schwing (1987) or Xu & Helou (1996), of which at most 20 % comes from the $11.3 \mu\text{m}$ band. The rest must be essentially continuum emission, to be compared with an average emission of $\simeq 1$ mJy/pixel in the LW3 filter (12.0 – $18.0 \mu\text{m}$). Although the result of this comparison is encouraging, it would be premature to try to extract the spectral slope of the continuum from these very rough numbers.

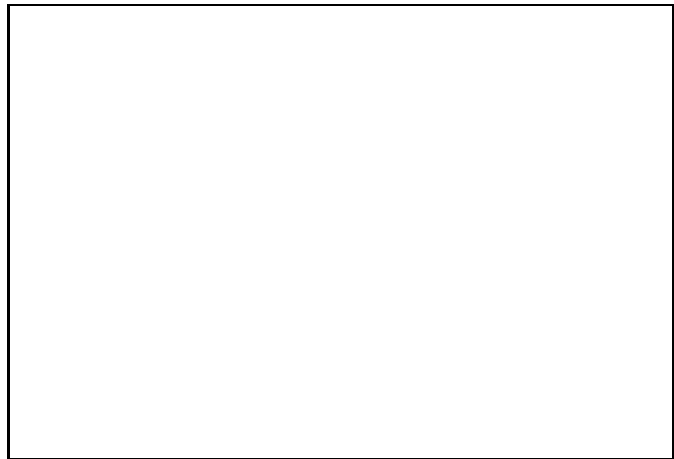


Fig. 12. Average differential spectra in Field c of Fig. 1, an active star–forming region of the ring of M 31, with three different selections of pixels. The middle and top spectra are shifted vertically for clarity. Top: pixels strong in the $11.3 \mu\text{m}$ band and weak in the 6.2 and $7.7 \mu\text{m}$ ones. Middle: pixels strong in all three bands. Bottom: pixels strong in the $6.2 \mu\text{m}$ band and weak in the $11.3 \mu\text{m}$ one. The latter spectrum resembles the usual Galactic AIB spectra. A continuum obtained from the pixels with no visible emission in any of the bands has been subtracted. Note that the continuum level and shape are lost in the process, as explained in the text

In order to clarify the situation in Field c, we present on Fig. 15 and 16 comparisons of the ISO filter maps with

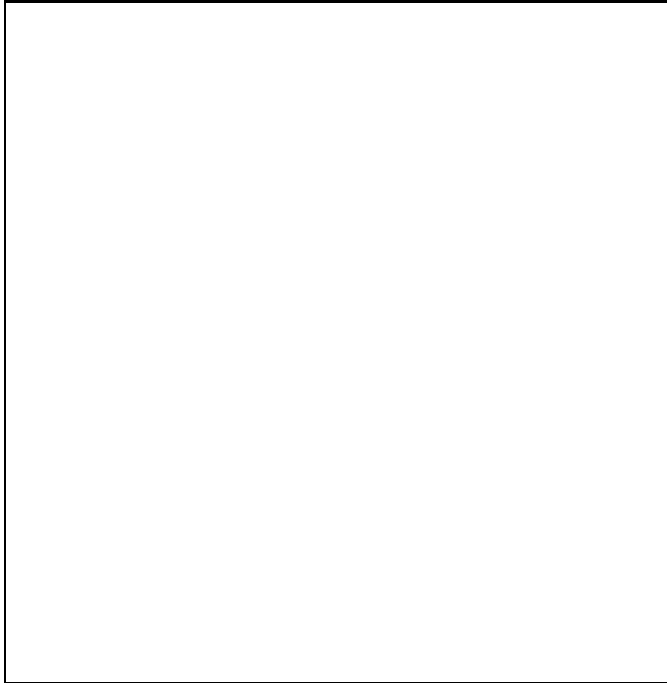


Fig. 13. Map of Field c of Fig. 1, an active star-forming region of the ring of M31 in the integrated $6.2 \mu\text{m}$ emission band (contours) superimposed on the LW2 filter ($5.0\text{--}8.0 \mu\text{m}$) image (grey scale, in units of $1 \text{ mJy per } 6''$ pixel). Coordinates are J2000. The LW2 point source at $00\text{h } 41\text{m } 05\text{s}, 40^\circ 36' 40''$ is a red Galactic star which has been used to recenter the CVF $6.2 \mu\text{m}$ image on the LW2 one. The field of the CVF is indicated by the dashed lines. Note the good correspondence between the two images, suggesting that the LW2 image is dominated by the AIBs

maps of other quantities. On Fig. 15, the HI column density and the CO(1–0) line intensity contours are superimposed on the LW3 image. We note the good overall correspondence between the mid-IR and the distribution of gas that we have already seen in the full maps of Fig. 4 and 5, especially at faint levels. However the strongest LW3 feature does not correspond to a peak in the gas distribution, but rather to the H II region PAV78 159. Fig. 16 compares the LW3 image with the LW2, H α and UV images. It shows that there are quantitative differences between the LW3 and the LW2 images. The correspondence is excellent at the faint levels but not so good at higher levels. The LW2 peak at $00\text{h } 40\text{m } 50\text{s}, 40^\circ 37' 20''$, not visible on the LW3 image and which coincides with a UV source, is a star. The H II regions seen in H α generally coincide with peaks in both the LW2 and LW3 maps as expected, while the correspondence is almost inexistent with the UV. We already remarked these properties at the scale of the ring of M31. Finally we note by comparing Fig. 14 and Fig. 16 that the regions where the $11.3 \mu\text{m}$ AIB dominates over the other AIBs do not seem poorer in UV.

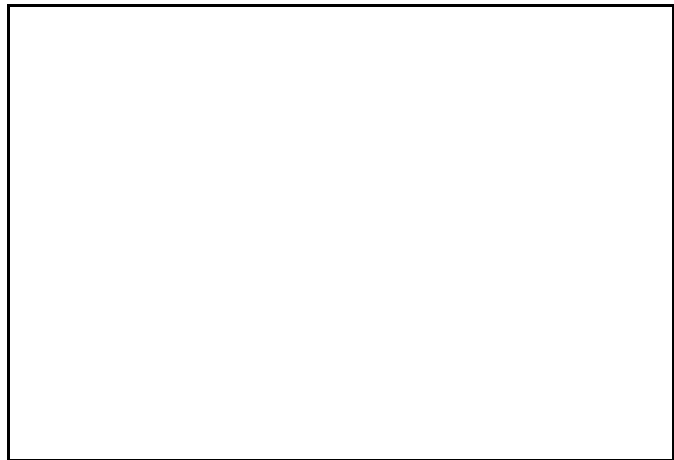


Fig. 14. Map of Field c of Fig. 1, an active star-forming region of the ring of M31, in the integrated $11.3 \mu\text{m}$ emission band (contours) superimposed on the LW3 filter ($12.0\text{--}18.0 \mu\text{m}$) image (grey scale). The average differential spectra for the $11.3 \mu\text{m}$ -strong pixels of three strips in the CVF image are displayed on the right of the figure. Note in particular that the $11.3 \mu\text{m}$ emission regions of the lower-left strip, which do not correspond to strong peaks in the LW3 map, do not produce a detectable emission in the $6.2, 7.7$ and $8.6 \mu\text{m}$ bands

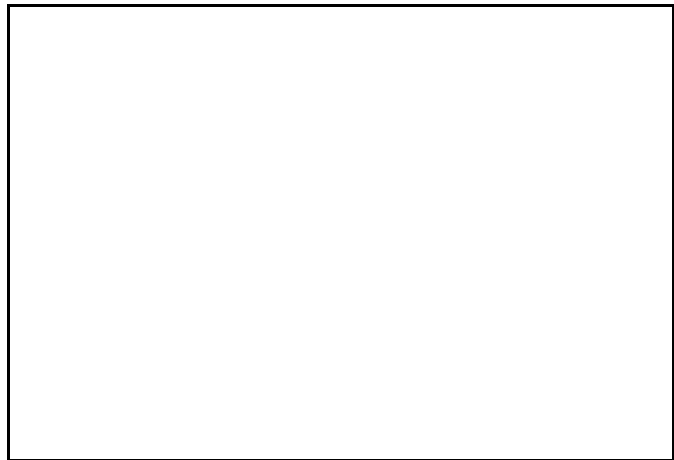


Fig. 15. Map of Field c of Fig. 1, an active star-forming region of the ring of M31 in the LW3 filter ($12.0\text{--}18.0 \mu\text{m}$) (color; unit = 1 mJy/pixel). The white contours are for the 21-cm line integrated intensity, from data in Brinks & Shane (1984): levels from 1000 to 3500 K km/s^{-1} in steps of 500 K km/s^{-1} . The red contours indicate the intensity of the CO(1–0) line map from Loinard et al. (1999): contour levels 2 to 9 K km s^{-1} in steps of 1 K km s^{-1} . The angular resolution of the 21-cm map is $24'' \times 36''$, and that of the CO map is $45''$. The correspondence between the LW3 map and the distribution of gas is good as far as one can judge given the very different angular resolutions, except for the main LW3 peak which coincides with a H II region

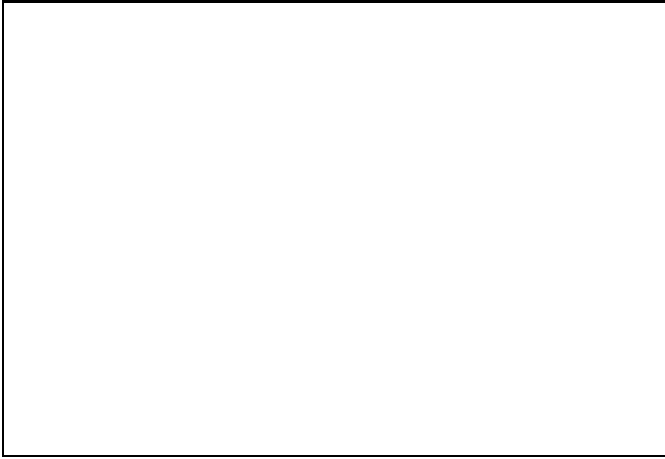


Fig. 16. Map of Field c of Fig. 1, an active star-forming region of the ring of M31 in the LW3 filter (12.0–18.0 μm) (color; unit = 1 mJy/pixel). The black contours are for the LW2 image (levels 1 to 4 mJy/pixel by steps of 1 mJy/pixel). The white contours are $\text{H}\alpha$ isophotes (levels 0.5, 1.5, 2.5, 5 and $7.5 \cdot 10^{-15}$ erg cm^{-2} s^{-1} per $2''$ pixel). The red contours are UV isophotes at 200 nm (levels 0.15, 0.175, 0.2 to 0.6 by 0.1, in units of $2.1 \cdot 10^{-17}$ erg cm^{-2} s^{-1} \AA^{-1} arcsec^{-2} ; the background is at 0.116 unit). The main H II regions ($\text{H}\alpha$ peaks) are in order of increasing right ascension PAV78 147, 152, 159, 157 (south of 159) and 161 (Pellet et al. 1978). Coordinates are J2000. The main UV peak at 00h 40m 55s, $40^\circ 36' 10''$ is a hot star or stellar cluster, probably belonging to M31. It coincides with the 12 mag. star BGH88 40 2579 (Berkhuijsen et al. 1988) but is more probably to be identified with the UV object HIB95 82-12 (Hill et al. 1995) in spite of a position difference of $14''$. Another peak at 00h 40m 50s, $40^\circ 37' 20''$ is very close to the emission-line object MLA93 270 (Meyssonnier et al. 1993) and to the red 13th mag. star BGH88 40 2486 (Berkhuijsen et al. 1988) so that the identification is unclear. Note the excellent correspondence between the LW2 and LW3 images at faint levels, but also the differences at higher intensities. There is little mid-IR emission in the UV-rich part of the field, and vice-versa. There are however LW2 and LW3 peaks in the direction of the H II regions, the strongest peak coinciding with PAV78 159 (Pellet et al. 1978)

8. Conclusions

In this paper, we have compared maps of the SW part of M31 at different wavelengths. In particular the mid-IR maps obtained with ISOCAM with the LW3 (12.0–18.0 μm) and the LW2 (5.0–8.0 μm) filters at a resolution of $6'' \times 6''$ have been compared with lower-resolution H I and CO maps, with a higher-resolution $\text{H}\alpha$ map and with a far-UV map at 200 nm with a resolution of $20''$ presented here for the first time. We also built smaller maps in the 6.2 μm and in the 11.3 μm AIB from ISOCAM CVF observations in a relatively active field of the star-forming ring, and compared them with other observations. The results of this study can be summarized as follows.

- The mid-IR emission is very well correlated with the column density of gas (atomic + molecular), but little with the $\text{H}\alpha$. We conclude from this observation that the emission is globally dominated in M31 by the diffuse ISM rather than by ISM at the interfaces between H II regions and neutral clouds.
- The mid-IR emission shows very little correlation with the far-UV radiation. This cannot entirely be due to extinction of the far-UV in regions emitting in the mid-IR. The existence of regions with similar gas column densities hence similar extinctions and with identical mid-IR emissions but very different UV intensities shows that the AIB carriers in M31 are not primarily excited by UV radiation except near star-formation centers. This confirms and extends the observation by Uchida et al. (1998) of a Galactic reflection nebula with little UV showing a “normal” AIB spectrum. In M31 like in this case, the excitation of the AIBs is dominated by something else than UV radiation, probably by photons in the visible. There is however some contribution of the UV to the excitation of the mid-IR emission that becomes apparent when the emission per H atom is plotted as a function of the UV flux (Fig. 9). In the disks of M31 and of the Galaxy the UV excitation becomes important when the UV radiation density is of the order of 2 times that near the Sun. This explains why the 5.0–8.0 μm emission per H atom does not differ by more than 30 % in M31 and Galactic cirruses in spite of the differences in the UV radiation density.
- The emission in the LW2 band (5.0–8.0 μm) is probably dominated by the AIBs at 6.2 and 7.7 μm , which whatever the emission mechanism are believed to be heated transiently by some quantum mechanism. The emission in the LW3 band (12.0–18.0 μm) is dominated by a continuum. In our Galaxy, this continuum has often be attributed to emission by very small carbonaceous grains heated in semi-equilibrium by UV photons. The ratio between the intensities in these two bands $I_\lambda(12.0\text{--}18.0 \mu\text{m})/I_\lambda(5.0\text{--}8.0 \mu\text{m})$ is very uniform over the observed part of M31, of the order of 0.8, except near star-formation regions. This points to very related excitation mechanisms.
- There are however a few localized regions with a larger $I_\lambda(12.0\text{--}18.0 \mu\text{m})/I_\lambda(5.0\text{--}8.0 \mu\text{m})$ ratio. These regions which are close to, but not coinciding with H II regions have the same properties as similar Galactic regions, and can be interpreted in the same way. They are probably photodissociation interfaces. In these regions, the radiation field is probably strong enough to heat the very small interstellar grains to temperatures such that they contribute strongly to the emission in the LW3

(12.0–18.0 μm) band.

- Cesarsky et al. (1998) have observed a strange mid-IR spectrum in four different regions of M31. It is characterized by a strong, broad emission band at 11.3 μm and faint bands at 6.2, 7.2 and 8.6 μm compared to Galactic spectra. The present paper confirms this property and shows that the regions that exhibit this particular type of spectrum are only vaguely related with the regions emitting in the LW2 and the LW3 filters, and are not related with the presence or absence of UV radiation either.

The present results have profound consequences on our knowledge of the mid-IR emission mechanisms in the interstellar medium. In particular, we found that the mid-IR emission of the Galactic cirrus is not dominated by UV excitation, but probably rather by visible photons, or perhaps by another mechanism related to H I that remains to be demonstrated. It is only in regions submitted to a substantially higher UV radiation field (with respect to the visible radiation field) that UV excitation becomes important. The ρ Ophiuchi cloud where the UV radiation density is about 10 times that in the Solar neighborhood (Abergel et al. 1996) is such a region.

The physical interpretation of our results is not easy and requires a detailed comparison of the properties of the mid-IR emission of the ISM in a wide variety of conditions of density, temperature and radiation field. This will be the subject of a future paper, and we refrain here from any such interpretation. However we wish to remark that the radiation field in M31 is rather unique amongst nearby spiral galaxies by its deficiency in UV, due to its low star-formation rate even in the “star-forming ring” at 10 kpc from its center (M81 might be a similar case, but has been much less studied). The strange mid-IR properties of M31 (the existence of spectra with a broad 11.3 μm band and little emission in the 6.2, 7.7 and 8.6 μm bands) might be related to this lack of UV. It will be of particular interest to look for mid-IR spectra or filter observations of other objects with little UV radiation, either in the archives of ISO or with future infrared space facilities. The central regions of M31 are still poorer in UV than the region we have studied here. They are the subject of a paper in preparation. We have seen that the bulge of another spiral galaxy, NGC 7331, has properties similar to those of M31 (Smith 1998). On the other hand, as discussed by Cesarsky et al. (1998) the few available mid-IR spectra of elliptical galaxies, which are other UV-poor objects containing ISM, look “normal”, i.e. similar to those of Galactic objects. This might be connected with the idea that their ISM comes from recent cannibalism of S or Irr galaxies in which the mid-IR emitters had “normal” properties, contrary to M31.

Appendix: The interstellar radiation field in M31

From the visible surface photometry of M31 (Walterbos & Kennicutt 1987) and our UV surface photometry at 200 nm, one can roughly estimate the spectral energy distribution of the ISRF in the ring of M31.

The brightness in the V band in relatively unabsorbed regions of the 10 kpc ring is $I_V \simeq 22 \text{ mag. arcsec}^{-2}$ corresponding to $I_\lambda(550 \text{ nm}) \simeq 6 \cdot 10^{-18} \text{ erg cm}^{-2} \text{ s}^{-1} \text{ \AA}^{-1} \text{ arcsec}^{-2}$. We estimate the UV brightness along the same 21-cm line isophote of 1000 K km s^{-1} on each side of the 10 kpc ring. On the outer side (Fig. 4, yellow box 2) it is $1.2 \cdot 10^{-18} \text{ erg cm}^{-2} \text{ s}^{-1} \text{ \AA}^{-1} \text{ arcsec}^{-2}$ and on the inner side (Fig. 4, yellow box 1) it is $0.3 \cdot 10^{-18} \text{ erg cm}^{-2} \text{ s}^{-1} \text{ \AA}^{-1} \text{ arcsec}^{-2}$. Hence $I_\lambda(200 \text{ nm})/I_\lambda(550 \text{ nm}) \simeq 0.20$ on the outer side and 0.05 on the inner side. Note that extinction does not affect much the UV/visible ratios at this column density. The column density of H I is $1.835 \cdot 10^{21} \text{ H-atom cm}^{-2}$ corresponding to an total extinction through the disk of 2.9 mag. at 220 nm and 1.1 mag. at 550 nm, assuming that the extinction law in M31 is the same as the Galactic one. The contribution of molecular clouds to the average extinction is small and is neglected here. If we assume for simplicity that the UV sources have the same distribution perpendicular to the plane as the dust responsible for extinction and that the visible emission comes from a considerably thicker disk, we calculate that the dereddened $I_\lambda(220 \text{ nm})/I_\lambda(550 \text{ nm})$ ratios are only 1.55 times larger than the observed ones.

In the “quiescent” Field d of the ring (see Fig. 1) the V-band brightness is $I_V \simeq 21.75 \text{ mag. arcsec}^{-2}$ corresponding to $I_\lambda(550 \text{ nm}) = 7.5 \cdot 10^{-18} \text{ erg cm}^{-2} \text{ s}^{-1} \text{ \AA}^{-1} \text{ arcsec}^{-2}$. The average UV brightness (Fig. 4, yellow box 3) is $0.25 \cdot 10^{-18} \text{ erg cm}^{-2} \text{ s}^{-1} \text{ \AA}^{-1} \text{ arcsec}^{-2}$. Hence $I_\lambda(200 \text{ nm})/I_\lambda(550 \text{ nm}) \simeq 0.03$. This is similar to the ratio in the central 20'' of M31 (Oke et al. 1981). The UV/visible ratio is probably more affected by interstellar extinction than in the previous regions. There is not only a column density of $2.2 \cdot 10^{21} \text{ H-atom cm}^{-2}$ of H I in Region 2 but also a substantial amount of molecular hydrogen. The dereddening correction factor is uncertain but cannot be much larger than 3, thus the dereddened $I_\lambda(200 \text{ nm})/I_\lambda(550 \text{ nm})$ ratio is also small, probably less than 0.1.

The $I_\lambda(200 \text{ nm})/I_\lambda(550 \text{ nm})$ ratio for the local Galactic ISRF is $\simeq 0.66$ from the calculations of Mathis et al. (1983, Table A3). By direct integration of the B and I band starlight and interpolation to 550 nm (Tables 35 and 36 in Leinert et al. 1998) and comparison with the ultraviolet ISRF of Gondhalekar et al. (1980, Fig. 6) we find $I_\lambda(200 \text{ nm})/I_\lambda(550 \text{ nm}) \simeq 0.63$, in excellent agreement with Mathis et al. (1983). This is considerably larger than the above ratios for the M31 ring. This ring is thus deficient in UV with respect to the Solar neighbourhood, which itself is not an active star-forming region. The ring of M31 is even more deficient in UV (with respect to the visible) than the reflection nebula vdB 133, which is probably the most UV-deficient Galactic object for which a mid-IR spectrum has been obtained. From the spec-

tral classification and absolute magnitudes of the exciting stars given by Uchida and the color-color relations of Fig. 1 of Fanelli et al. (1987) we find a ratio $I_{\lambda}(200 \text{ nm})/I_{\lambda}(550 \text{ nm}) \simeq 0.4$, slightly smaller than that in the Solar neighbourhood but definitively larger than in the ring of M 31.

The intensity of the ISRF in the visible is however of the same order in the ring of M 31 and in the Solar neighbourhood. From Tables 35 and 36 in Leinert et al. (1998) one can estimate that if seen from outside at the same inclination as M 31 (77°), the Solar neighbourhood would have almost exactly the same V brightness as the M 31 ring. The mean stellar brightness of the sky at galactic latitudes $b = \pm 13^\circ$ is $I_V \simeq 22.2 \text{ mag. arcsec}^{-2}$. Thus the brightness of the Solar neighbourhood seen at an inclination of 77° would be:

$$I_V(\text{SN}, 77^\circ) \simeq I_V + I_V (1 - \exp(-A_V)),$$

where A_V is the extinction through the half-galactic plane at latitude $b = \pm 13^\circ$. This extinction is about 1 magnitude from the average HI column density (Stark et al. 1992), thus

$$I_V(\text{SN}, 77^\circ) \simeq 21.8 \text{ mag. arcsec}^{-2},$$

instead of $22 \text{ mag. arcsec}^{-2}$ for the ring of M 31. As the UV/visible intensity ratio is smaller in M 31, the absolute UV radiation density is correspondingly smaller in M 31 than in the Solar neighbourhood. This might have something to do with the difference between the “normal” mid-IR spectrum of the Galactic cirruses (Mattila et al. 1996; Onaka et al. 1996) and the strange mid-IR spectrum of M 31.

Acknowledgements. We thank François Boulanger and Charly Ryter for illuminating discussions. We also thank the referee for comments and questions which helped us to improve the paper substantially.

References

- Abergel A., Bernard J.P., Boulanger F. et al. 1996, A&A 315, L329
- Baade W. 1963, *Evolution of stars and galaxies*, Harvard University Press, Cambridge, Mass.
- Baade W., Arp H. 1964, ApJ 139, 1027
- Berkhuijsen, E., Humphreys R.M., Ghigo F.D., Zumach W. 1988, A&AS 76, 65
- Block D.L., Elmegreen B.G., Stockton A., Sauvage M. 1997, ApJ 486, L95
- Brinks E., Shane W.W. 1984, A&AS 55, 179
- Boselli A., Lequeux J., Contursi A., et al. 1997, A&A 324, L13
- Boselli A., Lequeux J., Sauvage M., et al. 1998, A&A 335, 53
- Boulanger F., Péroul M. 1988, ApJ 330, 964
- Boulanger F., Abergel A., Bernard J.-P., et al. 1996 A&A 312, 256
- Cesarsky C.J., Abergel A., Agnès P. et al. 1996, A&A 315, L32
- Cesarsky D., Lequeux J., Abergel A., et al. 1996a, A&A 315, L305
- Cesarsky D., Lequeux J., Abergel A., et al. 1996b, A&A 315, L309
- Cesarsky D., Lequeux J., Pagani L., et al. 1998, A&A 337, L35
- Cesarsky D., Jones A., Lequeux J., Verstraete L. 1999, A&A submitted
- Coulais A., Abergel A. 1998, in *The Universe seen by ISO* (Paris, October 20–23), ESA SP-427, in press
- Désert F.-X., Boulanger F., Puget J.-L. 1990, A&A 264, 610
- Devereux N.A., Price R., Wells L.A., Duric N. 1994, AJ 108, 1667
- Digel S.W., Grenier I.A., Heithausen A., Hunter S.D., Thaddeus P. 1996, ApJ 463, 609
- Donas J., Deharveng J.M., Laget M., Milliard B., Huguenin D. 1987, A&A 180, 12
- Donas J., Milliard B., Laget M., 1991, A&A 252, 487
- Dumke M., Braine J., Krause M., et al. 1997, A&A 325, 124
- Fanelli M.N., O’Connell R.W., Thuan T.X. 1987, ApJ 321, 768
- Gondhalekar P.M., Phillips A.P., Wilson R. 1980, A&A 85, 272
- Helou G., Malhotra S., Beichman C.A. et al. 1996, A&A 315, L17
- Hill J.K., Isensee J.E., Bohlin R.C., et al. 1993, ApJ 414, L9
- Hill J.K., Isensee J.E., Bohlin R.C. et al. 1995, ApJS 98, 595
- Israël F.P., de Boer K.S., Bosma A. 1986, A&AS 66, 117
- Leinert Ch., Bowyer S., Haikala L. et al. 1998, A&AS 127, 1
- Loinard L., Dame T.M., Koper E., et al. 1996, ApJ 469, L101
- Loinard L., Dame T.M., Heyer M.H., Lequeux J., Thaddeus P. 1999, A&A in press
- Massey P., Armandroff T.E., Pyke R., Patel K., Wilson C.D. 1995, AJ 110, 2715
- Mathis J.S., Mezger P.G., Panagia N. 1983, A&A 128, 212
- Mattila K., Lemke D., Haikala L.K. et al. 1996, A&A 315, L353
- Meyssonnier N., Lequeux J., Azzopardi M. 1993, A&AS 102, 251
- Milliard B., Donas J., Laget M. 1991, Advances in Space Research 11, 135
- Moulinec H. 1989, Thesis, Université de Nice
- Neininger N., Guélin M., Ungerechts H., Lucas R., Wielebinski R. 1998, Nature 395, 871
- Oke J.B., Bertola F., Capaccioli M. 1981, ApJ 243, 453
- Onaka T., Yamamura I., Tanabe T., Roelling T.L., Yuen L. 1996, PASJ 48, L59
- Papoular R. 1999, A&A in press
- Pellet A., Astier N., Viale A., et al. 1978, A&AS 31, 439
- Reach W.T., Boulanger F. 1998, in *The Local Bubble and Beyond*, IAU Coll. 166, ed. D. Breitschwerdt, M.J. Freyberg, J. Truemper, Springer-Verlag, Heidelberg
- Rice W., Lonsdale C.J., Soifer B.T., et al. 1988, ApJS 68, 91
- Sauvage M., Blommaert J., Boulanger F. et al. 1996, A&A 315, L89
- Smith B.J. 1998, ApJ 500, 181
- Starck J.L., Abergel A., Aussel H., et al. 1999, A&AS 134, 135
- Stark A.A., Gammie C.F., Wilson R.W., et al. 1992, ApJS 79, 77
- Tran Quang Dan 1998, Thèse, Université Paris XI
- Uchida K.I., Sellgren K., Werner M. 1998, ApJ 493, L109
- Walterbos R.A.M., Kennicutt R.C., Jr. 1987, A&AS 69, 311
- Walterbos R.A.M., Schwing P.B.W. 1987, A&A 180, 27
- Xu C., Helou G. 1996, ApJ 456, 152

This figure "fg1.jpg" is available in "jpg" format from:

<http://arxiv.org/ps/astro-ph/9909347v1>

This figure "fg2.jpg" is available in "jpg" format from:

<http://arxiv.org/ps/astro-ph/9909347v1>

This figure "fg3.jpg" is available in "jpg" format from:

<http://arxiv.org/ps/astro-ph/9909347v1>

This figure "fg4.jpg" is available in "jpg" format from:

<http://arxiv.org/ps/astro-ph/9909347v1>

This figure "fg5.jpg" is available in "jpg" format from:

<http://arxiv.org/ps/astro-ph/9909347v1>

This figure "fg6.jpg" is available in "jpg" format from:

<http://arxiv.org/ps/astro-ph/9909347v1>

This figure "fg7.jpg" is available in "jpg" format from:

<http://arxiv.org/ps/astro-ph/9909347v1>

This figure "fg8.jpg" is available in "jpg" format from:

<http://arxiv.org/ps/astro-ph/9909347v1>

This figure "fg9.jpg" is available in "jpg" format from:

<http://arxiv.org/ps/astro-ph/9909347v1>

This figure "fg10.jpg" is available in "jpg" format from:

<http://arxiv.org/ps/astro-ph/9909347v1>

This figure "fg11.jpg" is available in "jpg" format from:

<http://arxiv.org/ps/astro-ph/9909347v1>

This figure "fg12.jpg" is available in "jpg" format from:

<http://arxiv.org/ps/astro-ph/9909347v1>

This figure "fg13.jpg" is available in "jpg" format from:

<http://arxiv.org/ps/astro-ph/9909347v1>

This figure "fg14.jpg" is available in "jpg" format from:

<http://arxiv.org/ps/astro-ph/9909347v1>

This figure "fg15.jpg" is available in "jpg" format from:

<http://arxiv.org/ps/astro-ph/9909347v1>

This figure "fg16.jpg" is available in "jpg" format from:

<http://arxiv.org/ps/astro-ph/9909347v1>